Exploring charge transport properties and functionality of molecule-nanoparticle ensembles

Devid, E.J.

3

Molecular devices based on molecule-gold nanoparticle arrays and networks

Here, I describe how molecule-gold nanoparticle arrays and networks are synthesized and characterized. Specifically, I present several synthesis routes to create gold nanoparticle arrays and networks functionalized with spin crossover molecules. Furthermore, the prime measurement techniques and setups are introduced here. These include basic charge transport measurements as well as optical analysis methods (UV-Vis spectroscopy and Raman spectroscopy). The latter provide information about the presence and properties of the molecules of choice in the network devices.

3.1 The synthesis of 2D molecule-metal nanoparticle arrays

Molecule-gold nanoparticle arrays and networks offer a variety of possibilities. By interfacing chemically tailored molecules [1] in between the metal nanoparticles, their physical properties [2, 3, 4] can in principle be tuned, e.g. to incorporate switchability. To synthesize molecule-gold nanoparticle arrays I have used a method adapted from L. Bernard *et al.* [5]. Basically, I synthesize a 2D molecule-metal nanoparticle array in a three-stage process. The first part is the synthesis of monodisperse gold nanoparticles in an aqueous solvent. The second part is the use of solvent exchange to change the polarity of the colloidal dispersion and to functionalize the gold nanoparticles by organic molecules. The third part incorporates another step of solvent exchange, to obtain apolar colloidal dispersions. Such a dispersion can then be used, by Langmuir methods [2], to have a 2D molecule-metal nanoparticle array self-assembled.

After obtaining a 2D molecule-metal nanoparticle array through self-assembly, several methods can be used to electrically contact the array. In addition, molecular exchange [6] (also called ligand substitution reactions [7, 8, 9]) can subsequently be performed.

3.1.1 Part 1: synthesis of gold nanoparticles in aqueous solvent

The method of preparing gold nanoparticles in an aqueous solvent (one-phase synthesis) was devised by J. Turkevich *et al.* [10]. A sodium citrate solution was used as a reducing agent to produce gold nanoparticles from a $HAuCl_4$ hydrate solution under boiling temperatures. This method was optimized by J. Slot *et al*. [11] and G. Tsutsui *et al*. [12] to synthesize [2] gold nanoparticles of ~5 nm or larger (in diameter) in a charge stabilized dispersion. In this optimized synthesis method, the reduction of gold is performed via a mixture of trisodium citrate and tannic acid. Here the tannic acid has a fast reductive and protective (stabilizing) effect during the synthesis [13, 14]. The particle size of the gold nanoparticles is further influenced by tannic acid through the number of nucleation sites formed during the reduction of chloroauric acid in ultra pure water. The trisodium citrate is a slow reducing reactant. It reduces the formed amount of gold nuclei further near boiling temperatures to allow the growth of the gold nanoparticles. In this part and following parts of the synthesis only ultrapure water (type 1 water, 18.2 MΩcm, also referred to as Millipore water) is to be used.

The synthesis begins by preparing a 20 mL aqueous solution that contains 4 mL 1% (w/v) trisodium citrate and 0.08 mL 1% tannic acid. The second aqueous solution

contains 1 mL 1%(w/v) chloroauric acid in 80 mL ultrapure water. Both solutions are heated up to 60 °C for 2 minutes. Then the reducing solution is quickly added to the gold ion solution. The reactant mixture is heated up to 100 °C and a condenser is connected to the reactor to allow reflux of the water. Boiling is done for at least 10 minutes to make sure that the reaction is complete. Then the colloidal dispersion can be cooled down toward room temperatures. After the synthesis, the colloidal dispersion is stored in a fridge (~7 °C) for months. A ruby red charge-stabilized colloidal dispersion (~100 mL) of spherical gold nanoparticles (~10^{12} particles/mL) is obtained in water. Here the gold nanoparticles are stabilized by the tannic acid and aggregation is prevented among the charge-stabilized gold nanoparticles [14]. The diameter size of a gold nanoparticle is chosen to be near ~10 nm, to balance the effects of the charging energy E_C on the gold nanoparticles and to optimize the self-assembly of the gold nanoparticles into an array. The properties of a nanoparticle array will depend on the type of self-assembly method used [15, 16].

3.1.2 Part 2: functionalization of gold nanoparticles by molecules

In the second part of the synthesis of molecule-gold nanoparticle arrays, the gold nanoparticles (NP) will trade in its previous electrostatic stabilization by a steric stabilization. This is done by changing the polarity of the solvent in the gold nanoparticle dispersion via a solvent exchange. Next, thiolated molecules can be used as a capping ligand for the nanoparticles, to allow stabilization of the nanoparticle ensemble via steric hindrance.

The procedure starts as follows. First, centrifugation is performed on a desired volume of aqueous gold nanoparticle dispersion. After 15000 RPM (rotations per minute) cooled (10 ºC) centrifugation for 1 hour the gold nanoparticles have settled down. The supernatant (water) is removed and ethanol is added to redisperse the settled down gold nanoparticles. The dispersion is sonicated to yield a stable redispersion. The next step is to prepare a solution of alkane(mono)thiol molecules in (N_2 washed) ethanol with an (excess) concentration of 0.14 mol/L [16, 17]. This is done in a glovebox in a N_2 atmosphere. Octane(mono)thiol (C8) molecules (molecule length ~1.3 nm [5]) are used most, to later define stable gold nanoparticle-molecule(s)-gold nanoparticle junctions with a junction length of around 2 nm [2, 6, 18, 19]. The alkanethiol solution is added quickly to the redispersed gold nanoparticle dispersion. The mixed octanethiol-gold nanoparticle dispersion in a glass bottle (sealed with a screwable lid) is again sonicated

in a water bath for more than five minutes to further stimulate the capping of the gold nanoparticle surfaces by octanethiol molecules. In time the functionalized gold nanoparticles will aggregate and start to settle down. The sedimentation of the functionalized gold nanoparticles can be accelerated by cooling the dispersion via a refrigerator. After at least two days all the functionalized gold nanoparticles have settled down and a dark blue sediment lies on the bottom of the bottle [20].

3.1.3 Part 3: self-assembly of 2D alkanethiol-gold nanoparticle array

In the third and final part, the supernatant (ethanol) is first removed from the functionalized gold nanoparticles settled down on the bottom of the bottle. Then the particles are redispersed in chloroform ($CHCl_3$) [20]. This dispersion displays a ruby-red colour again and is ready for self-assembly of C8-gold nanoparticle arrays. The self-assembly of a 2D array (see Figure 3.1) is based on an adapted Langmuir-Schaefer (L-S) technique [20, 21, 22]. A chosen μL volume of a C8-gold nanoparticles dispersion is added on the water layer in a teflon hole. If done properly, a well-ordered C8-gold nanoparticle array self-assembles on the water surface. To create large arrays a low particle concentration (between 0.06 and 0.3 mg/mL) is used [20, 23, 24].

By using a microcontact printing method (see Figure 3.2) an array can be transferred to the desired substrate [2, 20, 22]. This works well when both the array and substrate surface are hydrophobic. Hydrophilic surfaces tend to give rise to buckling or tearing of the array during microcontact printing [21]. Working with patterned PDMS stamps gives the possibility to imprint desired patterns and lines of C8-gold nanoparticle arrays on various substrates (i.e. glass, quartz, etc.). Furthermore, multilayered networks can be produced. This is done by transferring and imprinting 2D self-assembled arrays multiple times on the same substrate surface [21]. Finally, the gold nanoparticle arrays on a substrate are dried with N_2 gas and stored in a dark and sealed environment.

After the C8-gold nanoparticle array is printed on a substrate, scanning electron microscopy (SEM) is used to check both the gold nanoparticles and the C8-gold nanoparticle array. Figure 3.3 shows that the method used is feasible to make long-range-order C8-gold nanoparticle arrays on a flat SiO_2-Si substrate. Small areas (sizes ~150 nm) show well-ordered arrays with local defects.

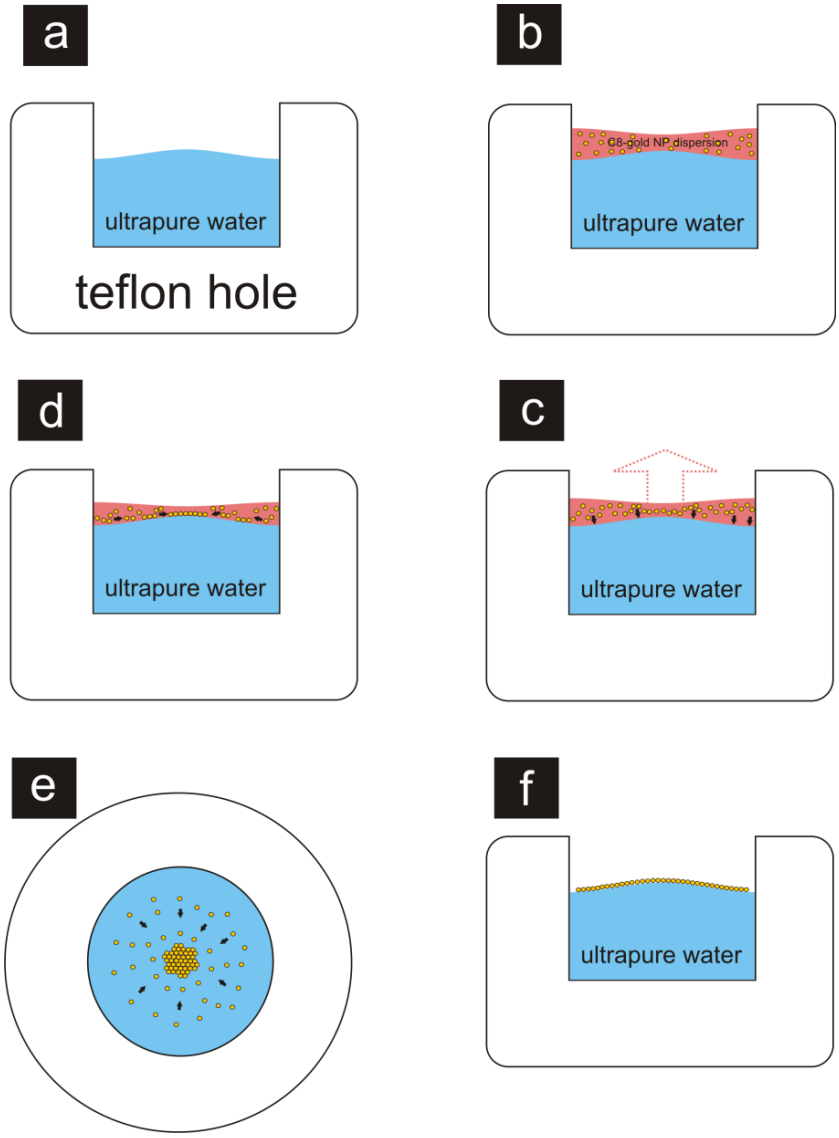

Figure 3.1: Schematics of the self-assembly of C8-gold nanoparticle (NP) array on an air-water interface. (a) A teflon model containing a hole in the middle filled with 300 µL ultrapure water containing a slight upward convex surface. (b) 30 µL C8-gold nanoparticle dispersion is added on the water to form a liquid lens surface. (c) The chloroform solvent is evaporating thereby concentrating the C8-gold nanoparticles. (d) The C8-gold nanoparticles go toward the air-water interface and form an initial self-assembled C8-gold nanoparticle array. (e) See schematic (d) from the top view perspective. (f) The self-assembly is complete and a 2D C8-gold nanoparticle array is formed floating on the water layer.

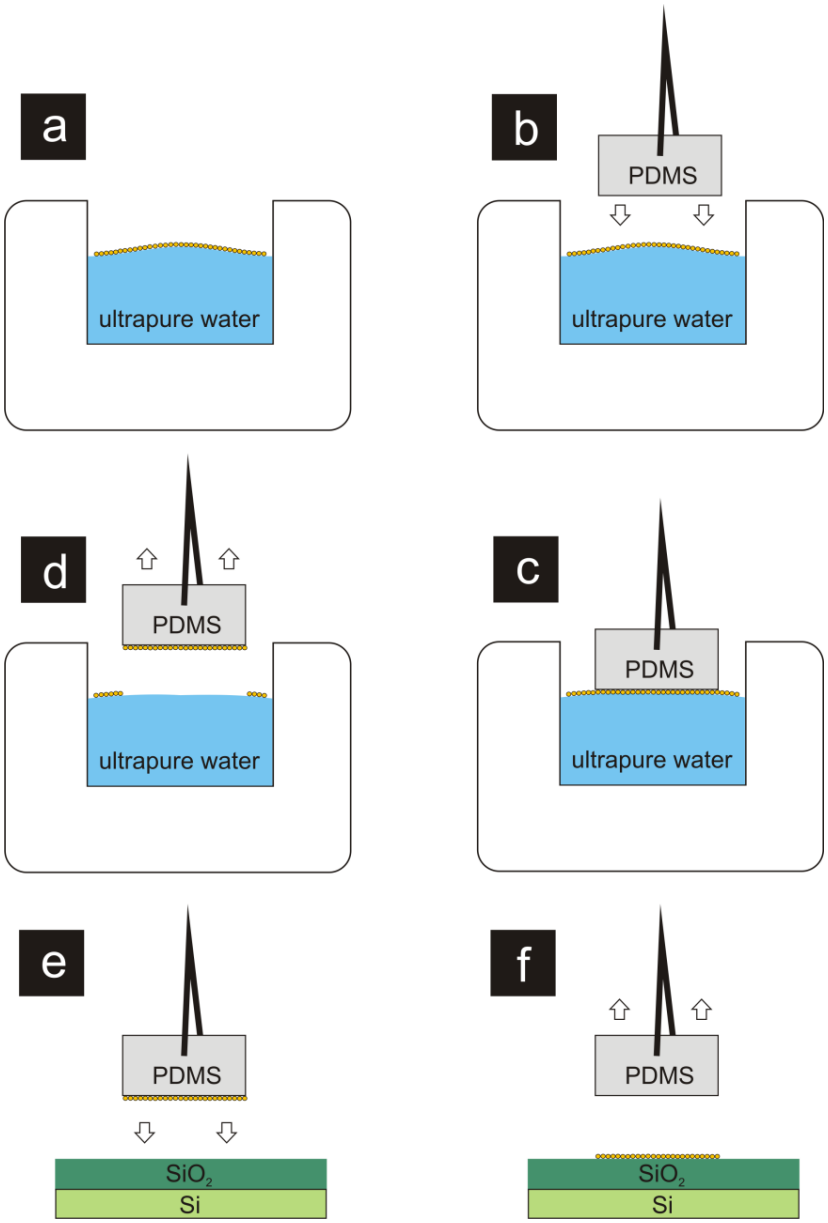

Figure 3.2: Schematics of microcontact printing of a self-assembled C8-gold nanoparticle (NP) array on an insulating SiO_2-silicon substrate. (a) The array on the water surface. (b) A PDMS stamp is picked up by tweezers to perform microcontact printing. (c) The stamp is put on top of the self-assembled array. (d) The stamp, containing the C8-gold nanoparticle array, is lifted up and dried with N_2. (e) The array is gently microcontact printed on the SiO_2-Si substrate (insulating SiO_2 layer ~200 nm thick). (f) The PDMS stamp is gently lifted up and the imprinted 2D array is inspected.

On larger length scales, however, boundaries between 2D grains can be observed.

The 2D alkanethiol-gold nanoparticle array opens several possibilities concerning tunability. By using different types of alkanethiol molecules one can tune the interparticle distance between the nanoparticles.

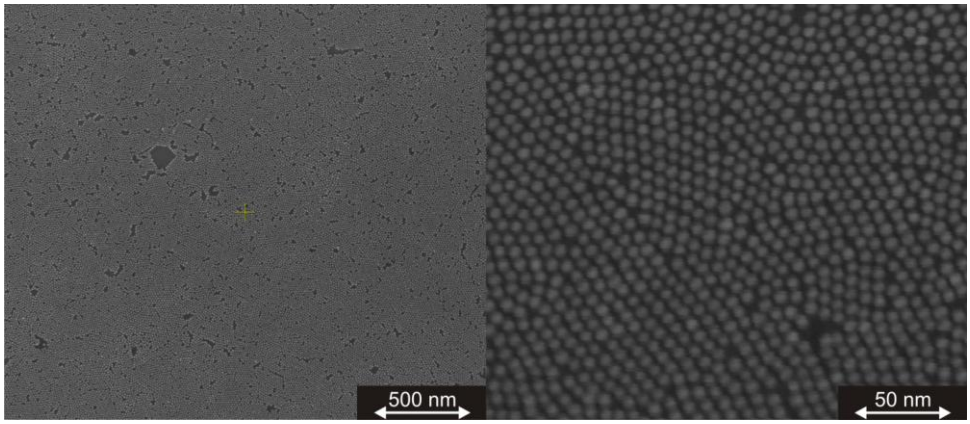

Figure 3.3: SEM images of a 2D C8-gold nanoparticle array that has been microcontact printed on SiO_2-Si substrate. The right image shows a zoom of the left image.

3.2 Molecular exchange

Molecular exchange (also called place-exchange [25] or ligand exchange [2]) is an alternative method to modify the functionalization of a gold nanoparticle surface. Molecular exchange involves the diffusion and chemical substitution of other species into capped-gold nanoparticle ensembles. Once molecular bridges are formed between the gold nanoparticle junctions the conductance properties of dithiol molecules can be studied.

The associative mechanism of molecular exchange is based on the following substitution reaction:

$$x(R`SH) + (RS)_m NP \rightarrow x(RSH) + (RS)_{m-x}(R`S)_x NP, \qquad (3.1)$$

where x and m represent the number of incoming and outcoming molecular species respectively and NP denotes a nanoparticle [8]. The rate of exchange depends on the concentration of both the incoming (R′-SH) and outgoing (R-SH) molecular species.

Furthermore, it is higher if the outgoing molecular species (i.e. alkanethiols) have shorter lengths. The exchange dynamics also depend on the temperature and the pH of the solvent used during the molecular exchange [26, 27, 28]. The exchange of molecular species can be confirmed via various analysis methods [6, 29, 30], including conductance measurements, as discussed below.

To illustrate this, we describe molecular exchange on octanethiol (C8)-gold nanoparticle networks. The molecular species to be inserted is Oligo(phenylene ethynylene)-dithiol (i.e. OPE), a benchmark molecular bridge. First, octanethiol networks are stamped onto a substrate (typically a nanotrench device, see paragraph 3.4 and a transparent substrate, see paragraph 3.5). After a series of conductance and optical measurements on the virgin samples, molecular exchange is carried out. For this, we use an OPE concentration of 0,5 mM in a 5:1 solution of pure tetrahydrofuran (THF) versus pure triethylamine (Et_3N). Here Et_3N is used as a deprotection agent to remove the protective acetate groups from OPE [31]. The molecular device is placed upside down (the C8-gold nanoparticle network is in contact with the OPE solution) while not touching the bottom of the glass jar. The molecular exchange is done in 24 hours. After 24 hours the exchanged molecular devices are extensively washed and rinsed with pure THF. The molecular devices are dried in a nitrogen atmosphere (i.e. in a glove box). Later they are further dried using nitrogen gas. With this, they are ready for another series of measurements, ranging from charge transport experiments to optical experiments.

3.3 Synthesis routes toward spin crossover-gold nanoparticle networks

One of the main goals of this thesis is to investigate the (charge transport) properties of spin transition molecules in a device structure, as introduced in Chapter 1. In this paragraph, I introduce three synthesis routes to prepare a spin crossover-gold nanoparticle network. Below, I describe all routes and discuss their possibilities and limitations.

3.3.1 Synthesis route 1: molecular exchange

The first synthesis route can be described as an indirect approach to make a spin crossover-gold nanoparticle array. Here, an alkanethiol-gold nanoparticle array is first

constructed (see section 3.1). Then this array is functionalized by spin crossover molecules through a molecular exchange process (see paragraph 3.2).

Octanethiol (C8) molecules are chosen to be used as spacer molecules in an alkanethiol-gold nanoparticle type of array. The interparticle distance in such an array is compatible with the length of a $Fe(S\text{-}BPP)_2$ molecule. The key step is then to design a process that is feasible for exchanging $Fe(S\text{-}BPP)_2$ molecules into a C8-gold nanoparticle ensemble. During molecular exchange of $Fe(S\text{-}BPP)_2$ molecules, no deprotection reagents can be used, in contrast to the case of OPE, because experiments have shown that deprotective reagents have detrimental effects and leads to breakdown of the $Fe(S\text{-}BPP)_2$ complex molecule. The solvent acetonitril (MeCN) (pure 99,9%) turns out to be the best candidate to dissolve the $Fe(S\text{-}BPP)_2$ molecules, while not detrimentally affecting the C8-gold nanoparticle ensemble on the nanotrench device.

Molecular exchange was carried out with a $Fe(S\text{-}BPP)_2$ concentration of 0,5 mM, dissolved in MeCN. The molecular device, containing a C8-gold nanoparticle network, is placed upside down in the $Fe(S\text{-}BPP)_2$ solution. The molecular exchange was done in 4 days (i.e. to allow the $Fe(S\text{-}BPP)_2$ molecule to lose its protective acetate groups from the sulphur anchor groups in MeCN when contacting the gold surface [31]). After this step, the network is extensively washed and rinsed with pure MeCN. These molecular devices are dried in the glove box with the use of pure nitrogen gas. In Chapter 6 we further elaborate on the properties of such networks.

3.3.2 Synthesis route 2: complexation via a ligand-nanoparticle network

In this second synthesis route I first synthesize a ligand-gold nanoparticle ensemble. Here, the ligand is S-(4-{[2,6-(bipyrazol-1-yl)pyrid-4-yl]ethynyl}phenyl)ethanethioate, hereafter called AcS-BPP. If we compare to the spin transition molecule of interest (see Figure 1.5, in Chapter 1), we see that the latter basically consist of two AcS-BPP that are connected via a Fe^{2+} ion. The strategy chosen here is based on this observation. First, we make networks capped with the ligands. Then, we insert Fe^{2+} ions. This may lead to local formation of spin transition bridges between neighbouring nanoparticles, the Fe^{2+} working as a 'glue' for nearby ligands. Note that in this route, no alkanethiols are used. This type of strategy has been performed earlier to cap terpy-functionalized phospholipid on lecithin vesicles and to connect them via iron(II)-directed complexation [32].

To directly functionalize the gold nanoparticles with S-BPP molecules, we heat up a solution of 14.5 mg of AcS-BPP molecules in 2 mL pure (absolute) ethanol (EtOH) to 70 ºC. The next step is to add the hot AcS-BPP ethanolic solution quickly into a warm (heated around 50 ºC) gold nanoparticle ethanolic dispersion. The functionalized S-BPP-gold nanoparticles will settle down by gravity during three days and they are saved in a cold, dark storage environment. To obtain self-assembled S-BPP-gold nanoparticle arrays on substrates, a procedure similar to the one in paragraph 3.1.3 is used (array formation on a water surface; stamping). In Chapter 5 we elaborate on the properties of S-BPP-gold nanoparticle arrays without Fe^{2+} ions.

Based on this concept two routines have been tested to learn if Fe^{2+} complexation in a S-BPP-gold nanoparticle array is actually possible.

The first is to perform the self-assembly of a S-BPP-gold nanoparticle array in a diluted Fe^{2+} solution, instead of in pure Millipore water. The idea is that during self-assembly of the S-BPP-gold nanoparticles, the Fe^{2+} ions can be 'grabbed' by the nitrogen atoms of a S-BPP molecule. Another S-BPP-gold nanoparticle may contact the Fe(S-BPP)-gold nanoparticle, resulting in direct complexation. Unfortunately, this routine turned out to be complicated. A main point of concern is that the self-assembly process of S-BPP-gold nanoparticles is disrupted when Fe^{2+} ion concentrations are used above 3.5 mM. It seems that above a certain Fe^{2+} ion concentration threshold the S-BPP molecules become saturated with Fe^{2+} ions. Thereby the polarity of the capping S-BPP molecules can be changed and this will hamper the self-assembly process of the S-BPP-gold nanoparticles into an array. Another observation is that the type of solvent used during this assembly step influences the structuring of a S-BPP-gold nanoparticle ensemble. I have experimented with hot ethanol and acetonitril solvents. When synthesizing the S-BPP-gold nanoparticles in acetonitril solvents, the self-assembly process gives an ensemble that appears strongly three dimensional (3D), as seen in Figure 3.4. Importantly, Figure 3.4 shows that the gold nanoparticles are not aggregated. Figure 3.5 shows an ensemble obtained using hot ethanol solvent.

Unfortunately, several areas on top of the ensemble appear to be covered by a darkish layer (see right dark area on the left zoomed out SEM image of Figure 3.5). This is presumably a layer of cross-linked S-BPP molecules that is possibly mediated by Fe^{2+} ions. Figure 3.5 (the right zoomed in SEM image) displays a close packed gold nanoparticle structure. Apparently the type of solvent can affect the linking between

the S-BPP molecules (via the Fe^{2+} ions) during the self-assembly of the capped gold nanoparticles.

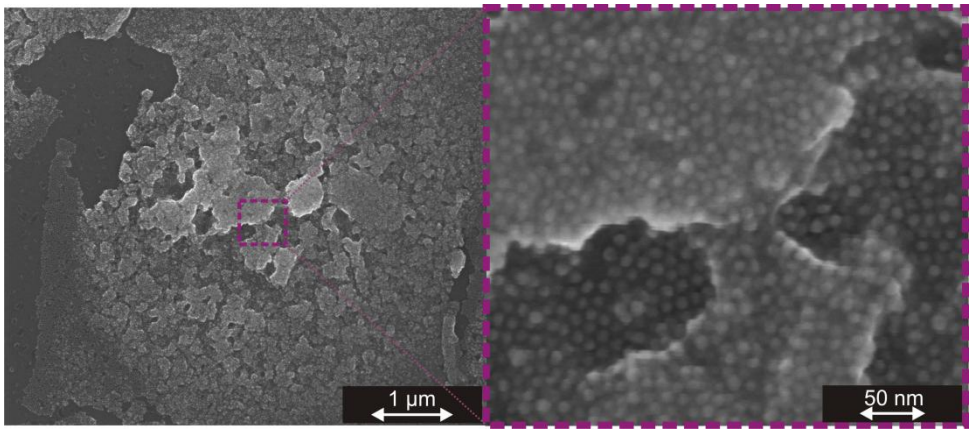

Figure 3.4: (left image) SEM image of S-BPP-gold nanoparticle ensemble (prepared via MeCN solvent and self-assembled with the presence of Fe^{2+} ions (i.e. 0.1 mM solution of Iron(II) perchlorate hydrate in Millipore water)). (right image) A zoom in on the 3D gold nanoparticle ensemble structuring, composed of several layers of non-aggregated gold nanoparticles. This ensemble is microcontact printed on (oxidized) silicon substrate.

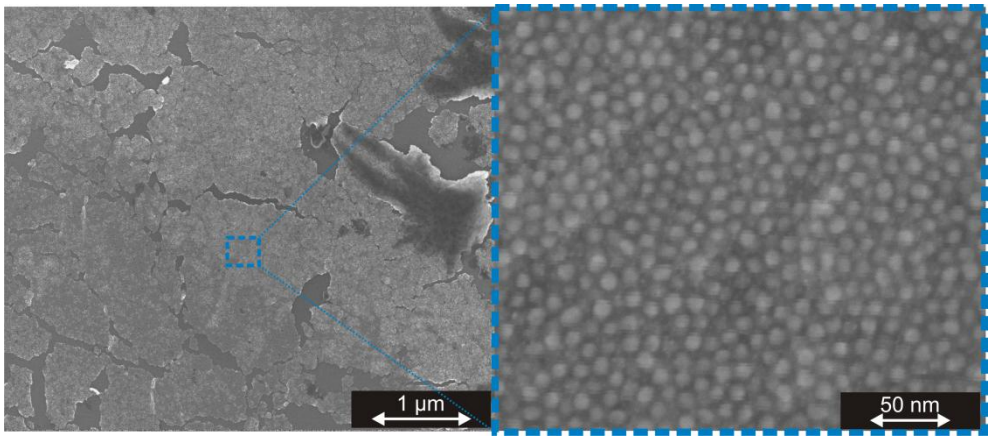

Figure 3.5: (left image) SEM image of S-BPP-gold nanoparticle ensemble (prepared via ethanol solvent and self-assembled with the presence of Fe^{2+} ions (i.e. 0.1 mM solution of Iron(II) perchlorate hydrate in Millipore water)). (right image) A zoom in on the hard, brittle ensemble of close packed non-aggregate S-BPP-gold nanoparticles. This ensemble is microcontact printed on (oxidized) silicon substrate.

The second routine is to perform Fe^{2+} ion exchange of a S-BPP-gold nanoparticle array already microcontact printed on a substrate. Here, a S-BPP-gold nanoparticle array is self-assembled on a Millipore water layer. This array is then microcontact printed on a substrate. The final step is to exchange Fe^{2+} ions into the S-BPP-gold nanoparticle array. This is carried out by using a 0.5 mM concentration of Iron(II) perchlorate hydrate in a (weak) polar solvent (i.e. ethanol or acetonitril). The exchange is done in 4 days. The array obtained is then washed and rinsed with the same type of pure solvent and dried in a glove box with nitrogen gas.

Unfortunately, room-temperature conductance experiments on arrays obtained via both routines above indicate very large resistances (above 100 GOhm). This has hampered the use of these samples.

3.3.3 Synthesis route 3: direct synthesis of $Fe(S\text{-}BPP)_2$ molecules with gold nanoparticles

Finally, I elaborate on a third synthesis route to obtain a $Fe(S\text{-}BPP)_2$-gold nanoparticle array. Here, full $Fe(S\text{-}BPP)_2$ molecules are used to bridge directly between gold nanoparticles. Neither alkanethiols nor S-BPP molecules are used in this procedure.

In short, a $Fe(S\text{-}BPP)_2$ solution with a concentration of 1 mM to 1.3 mM is prepared in pure methanol (MeOH). The temperature of the $Fe(S\text{-}BPP)_2$ solution in methanol can be elevated toward 40 °C till 50 °C to accelerate dissolving of the $Fe(S\text{-}BPP)_2$ molecules and to deprotect the thiol anchoring groups of the molecules. Also the gold nanoparticles are dispersed in a methanol solvent. Functionalization of the gold nanoparticles starts when the $Fe(S\text{-}BPP)_2$ solution is added to the gold nanoparticle dispersion. The functionalized $Fe(S\text{-}BPP)_2$-gold nanoparticles will settle down and the dispersion is saved in a cold, dark storage environment. After three days all the $Fe(S\text{-}BPP)_2$-gold nanoparticles have settled down. The synthesis of self-assembled $Fe(S\text{-}BPP)_2$-gold nanoparticle arrays can be continued in a way similar described in paragraph 3.1.3.

A limitation of these self-assembled $Fe(S\text{-}BPP)_2$-gold nanoparticle arrays (self-assembled on a water layer) is that microcontact printing via PDMS stamps fails. I suspect that this $Fe(S\text{-}BPP)_2$-gold nanoparticle array is more polar compared to other types of apolar molecule-gold nanoparticle arrays. The polarity of the $Fe(S\text{-}BPP)_2$

molecules appears to detrimentally affect the attachment of the Fe(S-BPP)$_2$-gold nanoparticle array on a PDMS stamp.

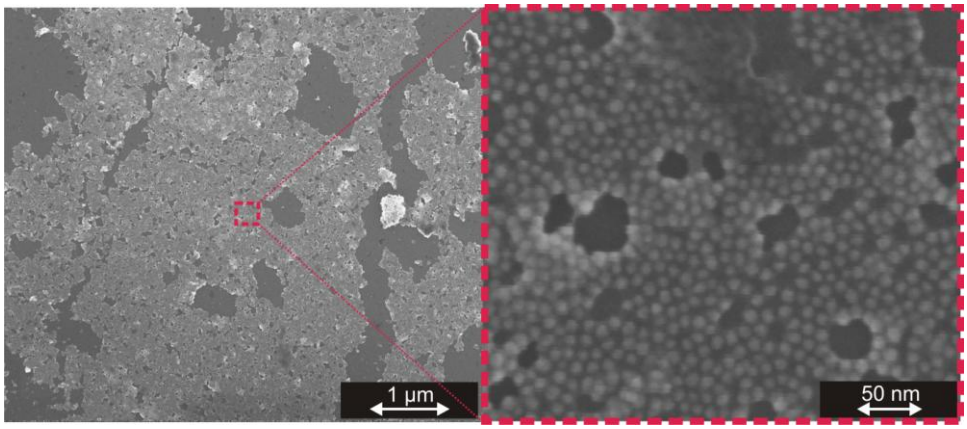

Figure 3.6: (left image) SEM image of Fe(S-BPP)$_2$-gold nanoparticle array (prepared via methanol solvent). (right image) A zoom in on the fragmented non-aggregate gold nanoparticles separated by only Fe(S-BPP)$_2$ molecules.

Alternative techniques (like Langmuir Blodgett (i.e. dipping) etc.) are required to transfer a Fe(S-BPP)$_2$-gold nanoparticle array to a substrate. But these techniques can give rise to more fragmented array structures. Figure 3.6 shows the best attempt to partially transfer a Fe(S-BPP)$_2$-gold nanoparticle array to the (oxidized) silicon substrate via microcontact printing. Still this array is too fragmented to perform conductive measurements on it at room temperatures. A possible solution to obtain a better structured Fe(S-BPP)$_2$-gold nanoparticle array on a substrate is done via dropwise self-assemble techniques.

During this dropwise technique, first 20 µL Millipore water is pipetted on the surface of the (oxidized) silicon substrate. The next step is to pipette a 10 µL Fe(S-BPP)$_2$-gold nanoparticle dispersion (in $CHCl_3$ solvent) into the middle of the convex water drop. If done properly, the drop of Fe(S-BPP)$_2$-gold nanoparticles will go through the convex water drop. The Fe(S-BPP)$_2$-gold nanoparticle dispersion is then trapped in between the silicon substrate and the polar water drop above it. The $CHCl_3$ solvent will evaporate from the Fe(S-BPP)$_2$-gold nanoparticle dispersion and the Fe(S-BPP)$_2$-gold nanoparticles arrange themself orderly in between the substrate-water interface. Once

the water is evaporated, a $Fe(S\text{-}BPP)_2$-gold nanoparticle array is deposited on the substrate. However, this combined self-assembly and deposition technique needs further optimization before room-temperature conductive measurements can be performed on these dropwise $Fe(S\text{-}BPP)_2$-gold nanoparticle arrays.

For this reason, the samples used in Chapter 6 are based on the 'traditional' exchange method (i.e. synthesis route 1, see paragraph 3.3.1).

3.4 Charge transport measurements

To study their charge transport properties, devices are required that provide reliable electrical contacts with the arrays. We achieve this via high-aspect-ratio (HAR) nanotrench structures. These devices are made via a combination of optical lithography and electron beam lithography. As shown in Figure 3.7 they consist of two wide electrodes separated by a tuneable gap of 50-200 nanometer. The gap size between the electrodes of these devices can be controlled over a wide size range. The individual electrodes consist of an adhesion layer of around 3 nm thick Ti covered by a 47 nm thick layer of gold [33].

Room-temperature charge transport measurements are performed in a dedicated probe station within a Faraday cage. The resistances typically being high, we use a voltage source and measure the current in the circuit. Charge transport measurements are controlled via a Labview program and a National Instrument data acquisition DAQ-mx card (see Figure 3.8(a)). The current is converted via a low noise current-voltage convertor-amplifier with variable-gain of 10^3 to 10^{11} V/A (Femto DLPCA-200).

To demonstrate the effect of molecular exchange, we refer to Figure 3.9. It shows current-voltage (*I-V*) measurements on a molecule-gold nanoparticle network printed on a HAR nanotrench device at room temperature. The blue line shows data for a virgin octanethiol (C8)-based network. In red (see Figure 3.9), we show results for the same sample after molecular exchange with conjugated OPE molecules. A clear increase in the conductance is observed (the exact ratio fluctuates [5, 34]). Interestingly, a back-exchange process, in which octanethiol molecules are re-inserted (see Figure 3.9, in green), is possible as well.

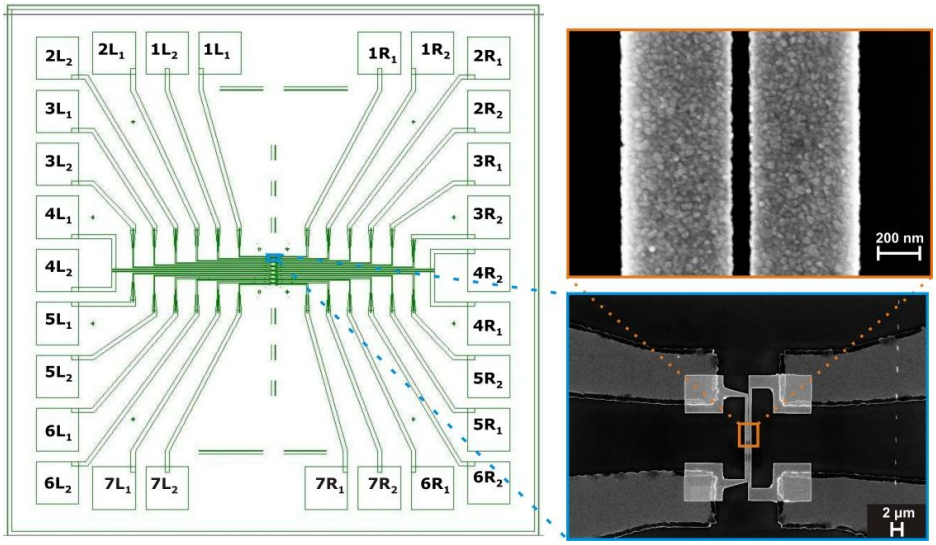

Figure 3.7: High-aspect-ratio nanotrench device onto which a molecule-gold nanoparticle array can be microcontact printed (in total 7 nanotrenches on one device). The gap between the gold electrodes can be 50-200 nm and the width of the electrodes can be as much as 10 µm.

After room-temperature characterization, charge transport measurements can be performed in the temperature range 1.5-325 K. This is done in a helium-based cryostat with a variable temperature insert (VTI) in Strasbourg. The devices are placed on a chip carrier, connected to a sample stick and then the whole dipstick is inserted in the cryostat (see Figure 3.8(b)). The DC electrical properties of the sample are measured using a semiconductor parameter analyzer (Agilent E5270B).

3.5 Optical properties of molecule-gold nanoparticle arrays

Exposing a 2D molecular-gold nanoparticle array to light, analytical information can be obtained about the properties of both the gold nanoparticles and the molecular species. Two types of optical techniques have been used here, namely ultraviolet (UV)-visible (Vis) spectroscopy and Raman spectroscopy. The first is used to analyze shifts in the surface plasmon absorbance of the nanoparticles. The second reveals information on (shifts of) vibrations of molecules in the molecule-gold nanoparticle ensemble.

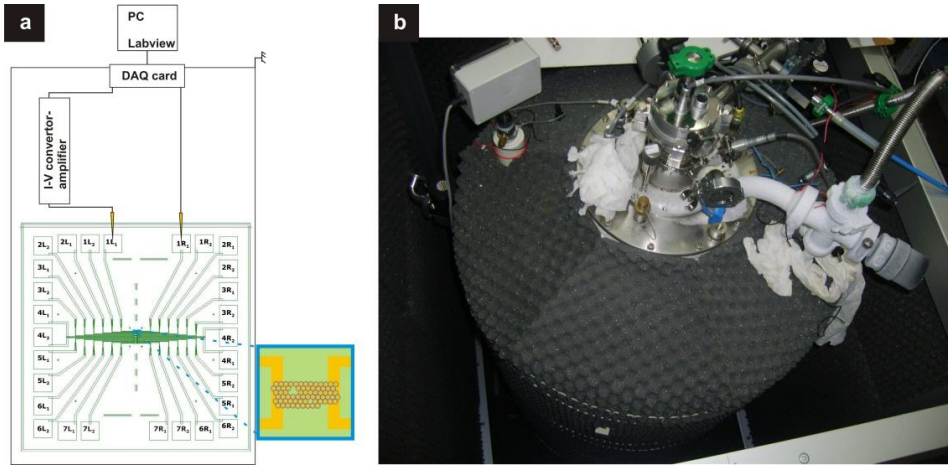

Figure 3.8: Setup used for measuring the electrical properties of molecular-gold nanoparticle ensemble devices. (a) Scheme of two-probe electrical measurement circuit used in Leiden for room-temperature measurements. (b) An image of the cryostat in Strasbourg (temperature range 1.5-325 K).

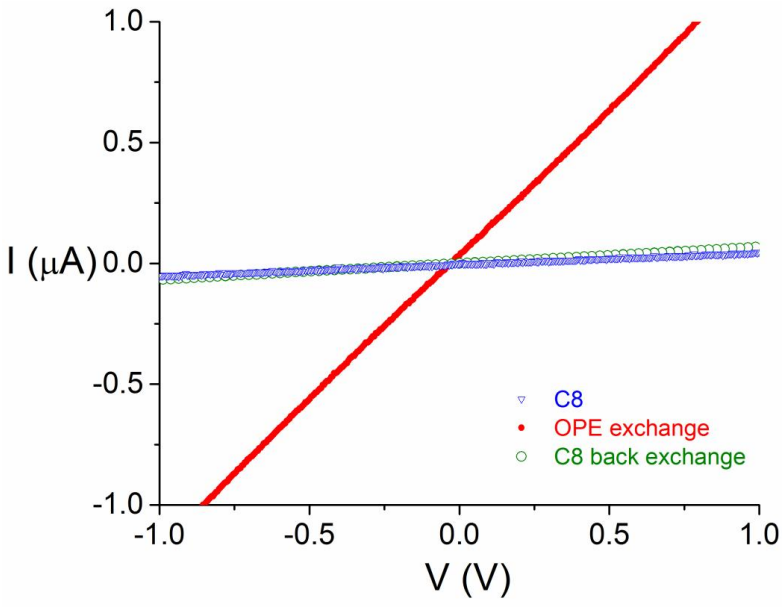

Figure 3.9: Room-temperature current-voltage (*I-V*) measurements on a C8-gold nanoparticle network (blue curve, $R \approx 21$ MΩ). This network can then later be exchanged with (OPE) molecules (red curve, $R \approx 0.8$ MΩ). Also on this same network, one can perform a back exchange with C8 molecules (green curve, $R \approx 15$ MΩ).

3.5.1 The surface plasmon resonance of a molecular-gold nanoparticle array

With UV-Vis spectroscopy, we can characterize the surface plasmon resonance (SPR) of gold nanoparticles, either in solution or in an array. This resonance comes about because the electric-field component of the incoming light wave induces a polarization of the free conduction electrons at the particle surface (see Figure 3.10(a)) [4]. As the positive charges on the surface of a gold nanoparticle can be assumed static, a net charge difference occurs due to the electron cloud displacement. This will give rise to a restoring force, finally resulting in a dipolar oscillation of the electron cloud. For gold nanoparticles, this resonance is typically observed in the visible regime. However, the exact resonance wavelength depends sensitively on the surroundings of the individual nanoparticle, specifically on the molecular capping layer and the packing of the gold nanoparticles in the array (see Figure 3.10(c)). This makes UV-Vis spectroscopy a good probe to check if a molecular exchange procedure has been successful [3].

To describe the interaction of light with metal nanoparticles, scattering theory was developed by Gustav Mie [35]. This theory describes the absorption and scattering of spherical particles based on the Maxwell equations. The main assumption of Mie theory is that both the surrounding molecular medium and gold nanoparticle are homogeneous and describable according to their bulk optical dielectric functions [4]. The optical absorption cross-section σ of the nanoparticles is calculated via equation 3.2:

$$\sigma = 12\pi\frac{\omega}{c}\varepsilon_m^{3/2}R^3\frac{\varepsilon_2(\omega)}{[\varepsilon_1(\omega)+2\varepsilon_m]^2+[\varepsilon_2(\omega)^2]}. \qquad (3.2)$$

Where ε_m is the permittivity of the surrounding medium (i.e. the real part) and $\varepsilon(\omega) = \varepsilon_1(\omega) + i\varepsilon_2(\omega)$ is the complex dielectric function of the cluster (i.e. the complex part) [5]. Note that equation 3.2 yields the resonance condition $\varepsilon_1(\omega) + 2\varepsilon_m = 0$, from which the resonance frequency (or frequencies) may be deduced.

The Mie theory is adequate in explaining the coupling of isolated spherical particles in an external field in the quasi-static regime (i.e. $\lambda >> 2r$, where r is the radius of the gold particle). However, Mie theory starts to break down when interactions between neighbouring gold nanoparticles are to be considered [3, 36]. This occurs approximately when $D \leq 5r$, where D represents the center-to-center distance between

the particles [4]. Coupling of the modes results in a red shift and broadening of the resonance. In this case, Maxwell-Garnett theory offers a more adequate description. This theory is used in Chapter 5.

Figure 3.10(b) displays the schematic experimental setup used for SPR measurements. A deuterium-halogen light source (for UV or Visible light respectively) illuminates a molecular-gold nanoparticle array, microcontact printed on a glass or quartz substrate, via an optical fiber. Via another fiber, the transmitted light is coupled into a spectrograph with a detector that can be cooled (to reduce thermal noise). Read-out is done by a pc. All the SPR measurements are performed in air at room temperature.

3.5.2 Surface-enhanced Raman scattering

Raman spectroscopy is a versatile analytical method for vibrational spectroscopy that allows one to analyze the chemical and structural composition of gases, liquids or solids [37, 38]. Unlike conventional infrared vibrational spectroscopy, Raman is a scattering method. The dominant form of optical scattering is Rayleigh scattering, where incident photons are elastically scattered from a molecule. Raman scattering is the inelastic scattering of photons by a molecule. The difference in frequency (i.e. wavelength) between the incident and scattered photons corresponds to vibrational quanta [39]. In accordance with the Raman selection rules (i.e. symmetry relates to Raman activity), the intensity of the Raman scattering is proportional to the magnitude of the change in molecular polarizability. So aromatic organic molecules will typically exhibit a more intense Raman scattering compared to aliphatic molecules [40].

For the Raman line intensity, one has

$$I_r \propto \nu^4 \sigma \mathrm{I}\ exp^{\left(-E_i/kT\right)}\ \mathrm{c.} \qquad (3.3)$$

Here I and ν represent the intensity and frequency respectively of the incident radiation. Furthermore, σ represents the Raman cross-section; $e^{-E_i/kT}$ is the Boltzmann factor for state i and c is the concentration of molecules [38]. The main limitation of Raman scattering is its sensitivity, that is low due to the low cross-section (~10^{-31} - 10^{-26} cm^2) of a molecule [38, 41]. Especially when the molecular adsorbate concentration in the sample is also low.

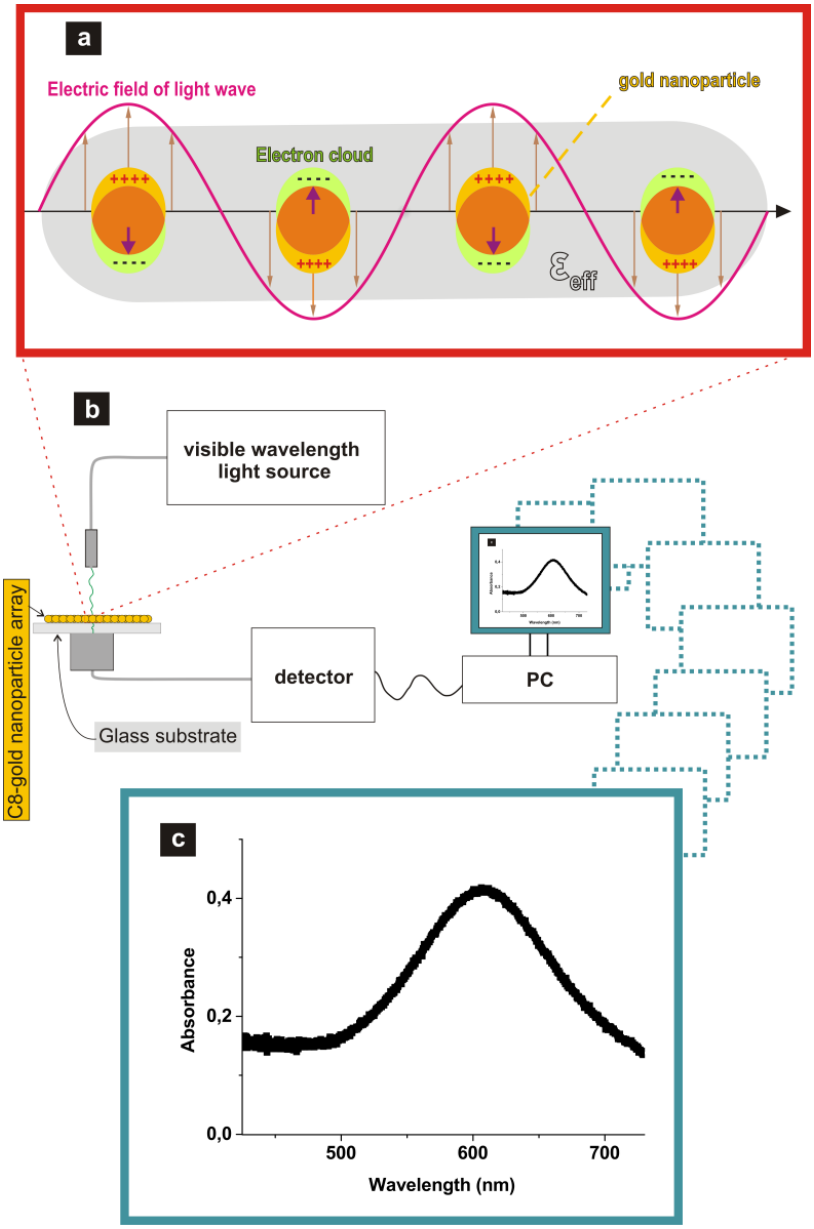

Figure 3.10: (a) Surface plasmon excitation of a gold nanoparticle (in the quasistatic regime) in a dielectric with permittivity ε_{eff}. (b) Scheme of the experimental setup to perform optical SPR measurements on molecular-gold nanoparticle arrays. (c) UV-Vis spectra of a microcontact printed C8-gold nanoparticle array on a glass substrate. The SPR peak is found around 608 nm.

In the 1970s, surface-enhanced Raman scattering (SERS) [4, 37, 38, 41-45] spectroscopy was introduced. With signal enhancements of several orders of magnitude, it allows for the analysis of samples containing minimal concentrations of molecular adsorbates on a nanostructured (noble) metal surface. The enhancement originates from both an electromagnetic (EM) effect and a chemical (CE) effect. The EM contribution stems from the increase in local electromagnetic fields due to resonant excitation of plasma oscillations (i.e. plasmon) in metal nanoparticles [40]. The CE contribution is related to the electronic properties of the molecules adsorbed on metal nanograins or particles. The presence of a metal nanoparticle may change the polarizability of the adsorbed molecules and this gives an increase in the Raman scattering efficiency [37].

The power of the SERS signal of molecules adsorbed onto metal nanoparticles (either in suspension or on a surface) is given by:

$$P_{SERS} = NI_L|\mathrm{A}(\mathrm{v_L})|^2|\mathrm{A}(\mathrm{v_S})|^2\sigma^{\mathrm{R}}_{\mathrm{ads}}. \quad (3.4)$$

Where I_L represents the intensity of the laser, N is the amount of molecules, σ^R_{ads}, is the effective Raman cross-section of the adsorbed molecular species [37]. The enhancement factors $|\mathrm{A}(\mathrm{v_L})|^2$ and $|\mathrm{A}(\mathrm{v_S})|^2$ represent the increase of the laser excitation and scattered fields respectively. Thus, EM enhancement involves the increase of both incident and Raman-scattered fields. At resonance, the laser beam excites the surface plasmons of a rough or curved noble metal surface. Due to the collective oscillations of conduction electrons a dipolar field (i.e. E_{SP}) will be emitted. At the surface of a gold nanoparticle, this induced dipolar field is related to the incoming laser field according equation 3.5:

$$E_{SP} = \left(\frac{\varepsilon-\varepsilon_0}{\varepsilon+2\varepsilon_0}\right) E_{laser} \left(\frac{r}{r+d}\right)^3. \quad (3.5)$$

Where ε is the dielectric constant of the metal and ε_0 is the dielectric constant of the external molecular medium. The interaction between the incoming electric field and the dipolar field will lead to a redistribution of electric field intensities in a region (i.e. a hot spot) near the gold nanoparticle. The magnitude of E_{SP} is further influenced by the decay distance around a spherical gold nanoparticle, where d is the distance of a single molecule separated from the surface of the gold nanoparticle (r is the particle radius again). The enhanced local field felt by the molecules, E_m, is the sum of the electric field magnitudes, i.e. $E_{SP} + E_{laser}$. The field enhancement $A(v)$ felt by the molecular adsorbate is then determined by the ratio of field amplitudes E_m/E_{laser}.

The amplitude of the SERS scattered field will be given by $E_{SERS} \propto |A(v_L)||A(v_S)|\, E_{laser}$. The SERS (EM) enhancement factor $G_{SERS}^{EM} = |A(v_L)|^2 |A(v_S)|^2$ becomes particularly strong when the real part of the ε is equal to $-2\varepsilon_0$ in equation 3.5. This is exactly the resonance condition for surface plasmons (cf. equation 3.2). In that case, small increases in the local field will produce large enhancements in the overall Raman scattering that approximately scales as E^4 [4, 37, 42, 43]. Any molecular adsorbate in proximity (i.e. a few nm) of the gold nanoparticle surface will feel an enhanced excitation intensity.

The second mechanism, namely CE enhancement, involves the electronic interaction between molecular adsorbate and the gold nanoparticle surface. CE enhancement relates to a mechanism called resonance Raman scattering. This describes how resonant intermediate states are created from new electronic states via charge transfer excitations between adsorbate and surface [42, 46]. These charge transfer excitations (i.e. either from the metal to the molecule or vice versa) can occur at about half the energy of the intrinsic intramolecular excitations of the molecular adsorbate [46]. The excited electrons can go from the filled molecular adsorbate orbitals to unfilled metal orbitals that lie above the Fermi level (i.e. molecule-metal charge transfer). Or the metal electrons can be excited to an empty lowest molecular adsorbate orbital (i.e. a metal-molecule charge transfer). These intermediate resonances cost less energy compared with intrinsic intramolecular excitations of the molecular adsorbate. Also the charge transfer processes may change the polarizability of the molecule and this will result in a change of the Raman scattering cross-section [47]. For example the polarizability of a ligand will change when it becomes coordinatively bonded to a metal transition.

Present-day SERS is a robust and effective analytical tool capable of combining and providing chemical information with single molecule sensitivity [4, 38-40]. Specifically, this thesis shows its great value for investigating molecule-nanoparticle networks.

Raman spectroscopy on molecular-gold nanoparticle arrays was carried out using a Horiba Jobin-Yvon LabRAM HR instrument with an Olympus confocal microscope (see Figure 3.11). The molecular-gold nanoparticle array was excited with a 632.8 nm HeNe laser or a 784.5 nm diode laser.

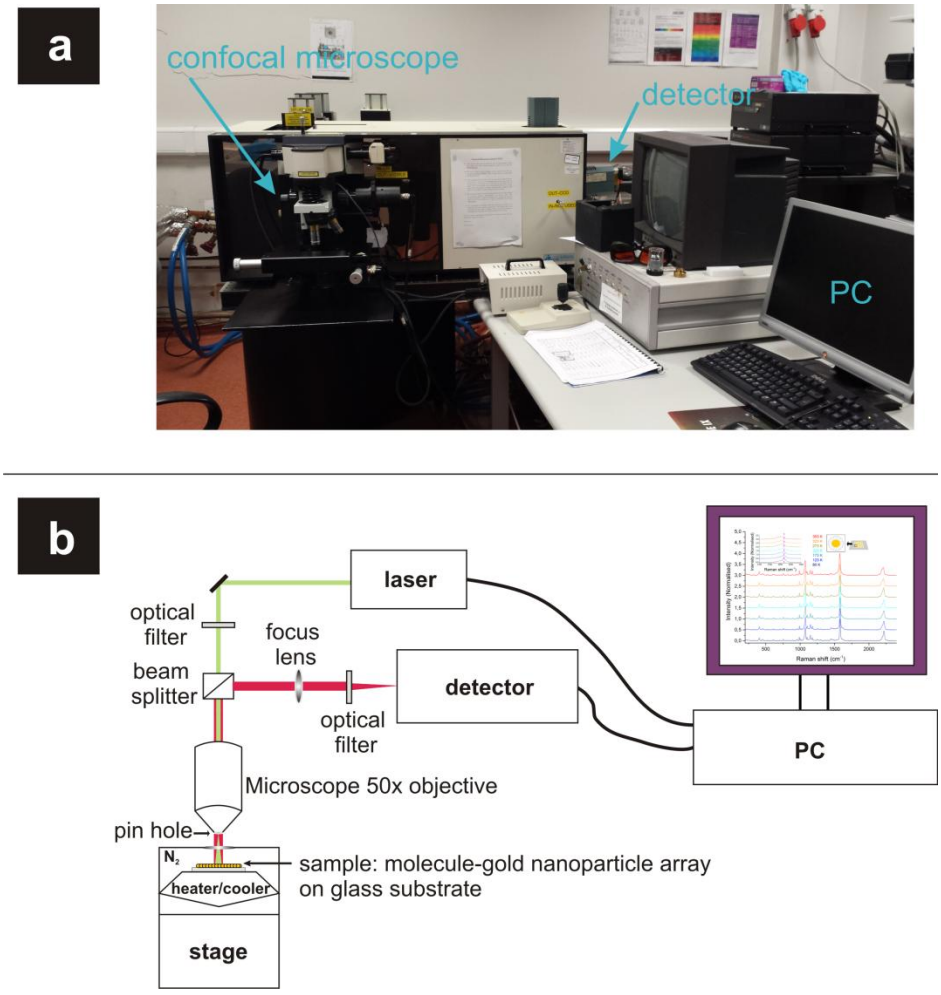

Figure 3.11: (a) An image of the Raman spectroscopy apparatus in Dublin. (b) A schematic of the Raman system in (a) used to perform variable temperature SERS measurements on a molecule-gold nanoparticle array.

An appropriate edge filter was put in the spectrometer depending on the excitation source. The laser was focused on a spot of approximately 3 µm with a 50x objective. A 300 µm confocal pinhole and a 600 lines per mm diffraction grating were employed, providing data at approximately 1 cm^{-1} resolution. The x-axis was calibrated versus the Rayleigh line (0 cm^{-1}) and the phonon mode from silicon wafer (520 cm^{-1}). Spectra were collected on a cooled 2D Andor CCD detector.

Temperature-dependent Raman measurements were performed on molecular-gold nanoparticle arrays from 77 K to 353 K in a nitrogen atmosphere. This was achieved by placing the molecular-gold nanoparticle array into a Linkam Scientific THMS600 temperature stage, which was cooled with liquid nitrogen. The desired temperature was set on the control unit and the sample was allowed to equilibrate for 30 minutes before measurement. An exposure time of 8 seconds was used with 5 accumulations for each spectrum. Three spectra were collected at each temperature and at different positions on the sample. The baseline of each spectrum was corrected using a polynomial fit with the Lab Spec software, before spectra were normalized to a temperature-independent peak. The three spectra for each temperature were then averaged.

Note: Dr. Ú. Prendergast performed the Raman spectroscopy experiments, while Professor Dr. T. E. Keyes did the SERS analyses of the samples (both are at DCU, Dublin). The samples discussed in this thesis were all made in Leiden.

3.6 References

1. J. C. Cuevas and E. Scheer, *Molecular Electronics: An Introduction to Theory and Experiment*, World Scientific, Singapore, **2010**.
2. A. Zabet-Khosousi and A.-A. Dhiran, Charge Transport in Nanoparticle Assemblies, *Chem. Rev.*, **108**, (2008), 4072-4124.
3. A. N. Shipway, E. Katz, and I. Willner, Nanoparticle Arrays on Surfaces for Electronic, Optical, and Sensor Applications, *Chemphyschem*, **1**, (2000), 18-52.
4. S. K. Ghosh and T. Pal, Interparticle Coupling Effect on the Surface Plasmon Resonance of Gold Nanoparticles: From Theory to Applications, *Chem. Rev*., **107**, (2007), 4797-4862.
5. L. Bernard, *Expanding the Horizon of Molecular Electronics via Nanoparticle Assemblies*. Ph. D. Thesis, University of Basel, Switzerland, **2006**.
6. J. Liao, L. Bernard, M. Langer, C. Schönenberger and M. Calame, Reversible Formation of Molecular Junctions in 2D Nanoparticle Arrays, *Adv. Mater*, **18**, (2006), 2444-2447.
7. M. J. Hostetler, S. J. Green, J. J. Stokes and R. W. Murray, Monolayers in Three Dimensions: Synthesis and Electrochemistry of ω-Functionalized Alkanethiolate-Stabilized Gold Cluster Compounds, *J. Am. Chem. Soc*., **118**, (1996), 4212-4213.
8. M. J. Hostetler, A. C. Templeton and R. W. Murray, Dynamics of Place-exchange Reactions on Monolayer-protected Gold Cluster Molecules, *Langmuir*, **15**, (1999), 3782-3789.
9. C. B. Murray, C. R. Kagan and M. G. Bawendi, Synthesis and Characterization of Monodisperse Nanocrystals and Close-packed Nanocrystal Assemblies, *Annu. Rev. Mater. Sci.*, **30**, (2000), 545-610.

10. J. Turkevich, P. C. Stevenson and J. Hillier, A Study of the Nucleation and Growth Processes in the Synthesis of Colloidal Gold, *Discuss. Faraday Soc.*, **11**, (1951), 55-75.
11. J. Slot and H. Geuze, A New Method for Preparing Gold Probes for Multiple Labeling Cytochemistry, *Eur. J. Cell. Biol.*, **38**, (1985), 87-93.
12. G. Tsutsui, S. J. Huang, H. Sakaue, S. Shingubara and T. Takahagi, Well-Size-Controlled Colloidal Gold Nanoparticles Dispersed in Organic Solvents, *J. Appl. Phys.*, **40**, (2001), 346-349.
13. H. Mühlpfordt, The Preparation of Colloidal Gold Particles Using Tannic Acid as an Additional Reducing Agent, *Experientia*, **38**, (1982), 1127-1128.
14. S. K. Sivaraman, S. Kumar and V. Santhanam, Room-temperature Synthesis of Gold Nanoparticles - Size-control by Slow Addition, *Gold Bulletin*, **43**, (2010), 275-286.
15. S. Datta, D. B. Janes, R. P. Andres, C. P. Kubiak and R. G. Reifenberger, Molecular Ribbons, *Semicond. Sci. Technol.*, **13**, (1998), 1347-1353.
16. X. M. Lin, H. M. Jaeger, C. M. Sorensen and K. J. Klabunde, Formation of Long-Range-Ordered Nanocrystal Superlattices on Silicon Nitride Substrates, *J. Phys. Chem. B*, **105**, (2001), 3353-3357.
17. H. B. Akkerman and B. de Boer, Electrical Conduction Through Single Molecules and Self-assembled Monolayers, *J. Phys.: Condens. Matter*, **20**, (2008), 013001(1-20).
18. L. Bernard, Y. Kamdzhilov, M. Calame, S. J. van der Molen, J. Liao and C. Schönenberger, Spectroscopy of Molecular Junction Obtained by Place Exchange in 2D Nanoparticle Arrays, *J. Phys. Chem. C*, **111**, (2007), 18445-18450.
19. C. M. Guédon, J. Zonneveld, H. Valkenier, J. C. Hummelen and S. J. van der Molen, Controlling the Interparticle Distance in a 2D Molecule-nanoparticle Network, *Nanotechnology*, **22**, (2011), 125205(1-5).
20. S. Huang, G. Tsutsui, H. Sakaue, S. Shingubara and T. Takahagi, Experimental Conditions for a Highly Ordered Monolayer of Gold Nanoparticles Fabricated by the Langmuir-Blodgett Method, *J. Vac. Sci. Technol. B*, **19**, (2001), 2045-2049.
21. V. Santhanam, J. Liu, R. Agarwal and R. P. Andres, Self-assembly of Uniform Monolayer Arrays of Nanoparticles, *Langmuir*, **19**, (2003), 7881-7887.
22. V. Santhanam and R. P. Andres, Microcontact Printing of Uniform Nanoparticle Arrays, *Nano Letters*, **4**, (2004), 41-44.
23. S. Huang, K. Minami, H. Sakaue, S. Shingubara and T. Takahagi**,** Effects of the Surface Pressure on the Formation of Langmuir-Blodgett Monolayer of Nanoparticles**,** *Langmuir*, **20**, (2004), 2274-2276.
24. S. Chen, Langmuir-Blodgett Fabrication of Two-dimensional Robust Cross-linked Nanoparticle Assemblies, *Langmuir*, **17**, (2001), 2878-2884.
25. J. Liao, M. A. Mangold, S. Grunder, M. Mayor, C. Schönenberger and M. Calame, Interlinking Au Nanoparticles in 2D Arrays via Conjugated Dithiolated Molecules, *New Journal of Physics*, **10**, (2008), 065019(1-7).
26. Y. Song and R.W. Murray, Dynamics and Extent of Ligand Exchange Depend on Electrical Charge of Metal Nanoparticles, *J. Am. Chem. Soc.*, **124**, (2002), 7096-7102.

27. R. L. Donkers, Y. Song and R. W. Murray, Substituent Effects on the Exchange Dynamics of Ligands on 1.6 nm Diameter Gold Nanoparticles, *Langmuir*, **20**, (2004), 4703-4707.
28. R. Hong, J. M. Fernandez, H. Nakade, R. Arvizo, T. Emrick and V. M. Rotello, In Situ Observation of Place Exchange Reactions of Gold Nanoparticles. Correlation of Monolayer Structure and Stability, *Chem. Comm.*, **22**, (2006), 2347-2349.
29. F. L. Leibowitz, W. Zheng, M. M. Maye and C.-J. Zhong, Structures and Properties of Nanoparticle Thin Films Formed via a One-step Exchange-Cross-Linking-Precipitation Route, *Anal. Chem*., **71**, (1999), 5076-5083.
30. A. C. Templeton, W. P. Wuelfing and R. W. Murray, Monolayer-protected Cluster Molecules, *Acc. Chem. Res*., **33**, (2000), 27-36.
31. H. Valkenier, E. H. Huisman, P. A. van Hal, D. M. de Leeuw, R. C. Chiechi and J. C. Hummelen, Formation of High-quality Self-assembled Monolayers of Conjugated Dithiols on Gold: Base Matters, *J. Am. Chem. Soc*., **133**, (2011), 4930-4939.
32. E. C. Constable, W. Meier, C. Nardin and S. Mundwiler, Reversible Metal-directed Assembly of Clusters of Vesicles, *Chem. Commun.*, (1999), 1483-1484.
33. J.-F. Dayen, V. Faramarzi, M. Pauly, N. T. Kemp, M. Barbero, B. P. Pichon, H. Majjad, S. Begin-Colin and B. Doudin, Nanotrench for Nano and Microparticle Electrical Interconnects, *Nanotechnology*, **21**, (2010), 335303(1-7).
34. C. M. Guédon, *Molecular Charge Transport: Relating Orbital Structures to the Conductance Properties*. Ph. D. Thesis, Leiden University, The Netherlands, **2012**.
35. G. Mie, Beiträge Zur Optik Trüber Medien, Speziell Kolloidaler Metallösungen, *Ann. Phys*., **25**, (1908), 377-445.
36. J. Wang, W. M. Lau and Q. Li, Effects of Particle Size and Spacing on the Optical Properties of Gold Nanocrystals in Alumina, *Journal of Applied Physics*, **97**, (2005), 114303(1-8).
37. K. Kneipp, Surface-enhanced Raman Scattering, *Physics Today*, **60**, (2007), 40-46.
38. U. K. Sur, Surface-enhanced Raman Spectroscopy Recent Advancement of Raman Spectroscopy, *Resonance*, **15**, (2010), 154-164.
39. P. L. Stiles, J. A. Dieringer, N. C. Shah and R. P. van Duyne, Surface-enhanced Raman Spectroscopy, *Annu. Rev. Anal. Chem*., **1**, (2008), 601-626.
40. C. L. Haynes, A. D. McFarland and R. P. van Duyne, Surface-enhanced Raman Spectroscopy, *Analytical Chemistry*, **77**, (2005), 338A-346A.
41. J. Popp and T. Mayerhöfer, Surface-enhanced Raman Spectroscopy, *Anal. Bioanal. Chem*., **394**, (2009), 1717-1718.
42. A. Campion and P. Kambhampati, Surface-enhanced Raman Scattering, *Chemical Society Reviews*, **27**, (1998), 241-250.
43. M. Moskovits, Surface-enhanced Raman Spectroscopy: a Brief Retrospective, *J. Raman Spectrosc*., **36**, (2005), 485-496.
44. D. L. Jeanmaire and R. P. van Duyne, Surface Raman Spectroelectrochemistry Part I. Heterocyclic, Aromatic, and Aliphatic Amines Adsorbed on the Anodized Silver Electrode, *J. Electroanal. Chem*. **84**, (1977), 1-20.
45. M. G. Albrecht and J. A. Creighton, Anomalously Intense Raman Spectra of Pyridine at a Silver Electrode, *J. Am. Chem. Soc*., **99**, (1977), 5215-5217.

46. A. Campion, J. E. Ivanecky III, C. M. Child, and M. Foster, On the Mechanism of Chemical Enhancement in Surface-enhanced Raman Scattering, *J. Am. Chem. Soc*., **177**, (1995), 11807-11808.
47. S. Schlücker, Surface-enhanced Raman Spectroscopy: Concepts and Chemical Applications, *Angew. Chem. Int. Ed*., **53**, (2014), 2-42.